C. R. Mecanique 345 (2017) 363–369

Contents lists available at ScienceDirect

Comptes Rendus Mecanique

www.sciencedirect.com

On the identifiability of the Hill-1948 model with one uniaxial tensile test

De l'identifiabilité du modèle de Hill-1948 à l'aide d'un seul essai de traction unixiale

Morgan Bertin, François Hild *, Stéphane Roux

LMT (ENS Paris-Saclay, CNRS, Université Paris-Saclay), 61, avenue du Président-Wilson, 94235 Cachan cedex, France

ARTICLE INFO

Article history:
Received 10 October 2016
Accepted 5 April 2017
Available online 24 April 2017

Keywords:
Digital Image Correlation (DIC)
Full field measurements
Identification
Plastic anisotropy

Mots-clés :
Corrélation d'images numériques (CIN)
Mesures de champ
Identification
Anisotropie plastique

ABSTRACT

A uniaxial experiment is performed on an ultra-thin specimen made of 17-7 precipitation hardened stainless steel. An anti-wrinkling setup allows for the characterization of the mechanical behavior with Integrated Digital Image Correlation (IDIC). The result shows that a single uniaxial experiment investigated via IDIC possesses enough data (and even more) to characterize a complete anisotropic elastoplastic model.

RÉSUMÉ

Un essai de traction uniaxiale est conduit sur un échantillon en acier inoxydable 17-7 à durcissement structural. Un montage anti-plissement permet la caractérisation du comportement mécanique par corrélation d'images numériques intégrée (CINI). Il est montré que ce seul essai analysé par CINI possède assez d'information (voire plus) pour une identification complète du modèle de plasticité anisotrope.

1. Introduction

For engineering design purposes, von Mises' [1] criterion is commonly used and gives satisfactory results. However, industrially-manufactured materials require plastic anisotropy to be accounted for. For instance, sheet metal forming calls for anisotropic plasticity models. Numerous authors have actively discussed their characterization. Whiteley [2] and Lloyd [3] investigated the importance of directionality in-deep drawing of sheet steel and so-called pressed-metals. Lankford et al. [4] proposed an experimental ratio to characterize plastic anisotropy. Hill [5] and Dorn [6] introduced the first models to

* Corresponding author.
E-mail address: hild@lmt.ens-cachan.fr (F. Hild).

http://dx.doi.org/10.1016/j.crme.2017.04.001

describe anisotropic plastic flows. These models have been extended to describe more complex constitutive laws [7]. Many developments have followed since these early propositions. However, one of the standard and most widely used models in nowadays commercial finite element codes [8] still is Hill's original proposition (i.e. the so-called Hill-1948 model [9]).

The calibration of such models calls for several tensile tests, at least in three directions (i.e. generally 0°, 90°, and 45° with respect to the rolling direction [10]). It is worth noting that more complex test configurations are also used (e.g., plain strain tensile test, shear test, experiment on cross-shaped samples, bulge test), even though very few of them are standardized. Most of these tests consider zones where the strain and stress states are uniform so that simple extraction techniques are considered to determine the sought quantities. With the development of full-field measurement techniques [11], another route consists in analyzing and designing the test as being fully heterogeneous [12].

The present study aims at identifying an anisotropic plasticity law, investigating Hill-1948 quadratic yield function via Integrated-DIC [13–19]. The key feature consists in analyzing a *single* sample made of ultra-thin precipitation hardened steel and tested in uniaxial tension. A sensitivity analysis is performed to assess the identifiability of an anisotropic yield surface coupled with linear kinematic hardening and isotropic elasticity. It will be shown that seven material parameters can be evaluated, even though the sample geometry remains very simple.

2. Methodological framework

2.1. Investigated constitutive law

In the following, linear and isotropic elasticity (with Young's modulus E and Poisson's ratio ν), and linear kinematic hardening with a quadratic yield criterion [5] are coupled. The total strain rate $\dot{\boldsymbol{\epsilon}}$ is written in terms of elastic and plastic strain rates $\dot{\boldsymbol{\epsilon}} = \dot{\boldsymbol{\epsilon}}_{\text{el}} + \dot{\boldsymbol{\epsilon}}_{\text{pl}}$, where $\dot{\boldsymbol{\epsilon}}_{el}$ is the elastic strain rate tensor and $\dot{\boldsymbol{\epsilon}}_{\text{pl}}$ the plastic strain rate tensor. As a first approximation, a linear kinematic hardening model is chosen for the back-stress rate [20] in which C is the hardening modulus. Last, the quadratic [5] anisotropic yield criterion is expressed in terms of rectangular Cartesian stress components as

$$f(\boldsymbol{\sigma}) = \sqrt{H_1(\sigma_{22}-\sigma_{33})^2 + H_2(\sigma_{33}-\sigma_{11})^2 + H_3(\sigma_{11}-\sigma_{22})^2 + 2H_4\sigma_{23}^2 + 2H_5\sigma_{31}^2 + 2H_6\sigma_{12}^2} \tag{1}$$

where H_i are constants expressed with the normal yield stress ratios (R_{11}, R_{22}, R_{33}) and those in shear (R_{12}, R_{23}, R_{31}) both with respect to the axes of anisotropy [9]

$$H_1 = \frac{1}{2}\left(\frac{1}{R_{22}^2} + \frac{1}{R_{33}^2} - \frac{1}{R_{11}^2}\right), \quad H_4 = \frac{3}{2R_{23}^2}$$
$$H_2 = \frac{1}{2}\left(\frac{1}{R_{33}^2} + \frac{1}{R_{11}^2} - \frac{1}{R_{22}^2}\right), \quad H_5 = \frac{3}{2R_{31}^2},$$
$$H_3 = \frac{1}{2}\left(\frac{1}{R_{11}^2} + \frac{1}{R_{22}^2} - \frac{1}{R_{33}^2}\right), \quad H_6 = \frac{3}{2R_{12}^2}$$

The computations being two dimensional, R_{31} and R_{23} are insensitive and set to 1 hereafter (and hence $H_4 = H_5 = 3/2$). One of the in-plane parameters must be chosen to decorrelate its value from the yield stress σ_y (i.e. H_1 is set to 1/2 in the sequel). Therefore, only three additional material parameters, i.e. H_2, H_3, and H_6, remain to be determined when plastic anisotropy is accounted for. To conclude, seven parameters (i.e. E, ν, σ_y, C, H_2, H_3, and H_6) need to be calibrated with the chosen model.

2.2. Integrated-DIC

The calibration of the material parameters $\{\boldsymbol{p}\}$ is performed via Integrated Digital Image Correlation, where the unknowns are no longer *kinematic* degrees of freedom, but the sought constitutive parameters *themselves*. Integrated-DIC is a global technique that registers an image f in the reference configuration and a series of N_t pictures g in the deformed configurations. Assuming gray level conservation, the inverse problem is solved by minimizing the sum of squared differences between the deformed images corrected by the trial displacement $\boldsymbol{u}(\boldsymbol{x}, t, \{\boldsymbol{p}\})$ and the reference image

$$\chi_f^2(\{\boldsymbol{p}\}) = \frac{1}{2\gamma_f^2 N_\Omega N_t} \sum_t \sum_\Omega ((g(\boldsymbol{x} + \boldsymbol{u}(\boldsymbol{x}, t, \{\boldsymbol{p}\}), t) - f(\boldsymbol{x}))^2 \tag{2}$$

with respect to $\{\boldsymbol{p}\}$. In this expression Ω denotes the Region of Interest (ROI), N_Ω its area in terms of the number of pixels it contains, $\boldsymbol{x}$ any considered pixel, and $\gamma_f = 323$ gray levels the standard deviation (i.e. 2% of the dynamic range of f) of the white noise assumed to affect each image independently (including the reference one, which is responsible for the factor of 1/2 coming as a multiplicative term in this functional). The load is also of importance for the identification because it increases the number of measured quantities and as a consequence diminishes the relative uncertainty by enhancing the material parameter sensitivities [12]. Thus, a second objective function, χ_F^2, is introduced

$$\chi_F^2 = \frac{1}{N_F N_t \gamma_F^2} \{\boldsymbol{F}_m - \boldsymbol{F}_c(\{\boldsymbol{p}\})\}^t \{\boldsymbol{F}_m - \boldsymbol{F}_c(\{\boldsymbol{p}\})\} \tag{3}$$

where $\{\boldsymbol{F}_m\}$ are the measured reaction forces and $\{\boldsymbol{F}_c(\{\boldsymbol{p}\})\}$ the computed levels that depend on the chosen material parameter set, N_F the number of load cells, and γ_F^2 the load variance (i.e. 100 N in the present case). The identification, which is based upon both observables (i.e. gray levels and reaction forces), is achieved by minimizing the global functional $\chi^2(\{\boldsymbol{p}\})$

$$\chi^2(\{\boldsymbol{p}\}) = \frac{N_\Omega}{N_\Omega + N_F} \chi_f^2(\{\boldsymbol{p}\}) + \frac{N_F}{N_\Omega + N_F} \chi_F^2(\{\boldsymbol{p}\}) \tag{4}$$

where the DIC and reaction force functionals have been introduced in Equations (2) and (3) respectively. The choice for the specific weight is issued from a Bayesian approach whereby the noise characteristics impose the appropriate weights to be given to quadratic differences [12]. In particular, quadratic differences are to be evaluated with a metric equal to the inverse noise covariance.

When nonlinear behaviors are investigated, the dependence of the displacement field with the material parameters is nonlinear as well. Consequently, sensitivity fields (i.e. displacement and reaction force derivatives with respect to the sought parameters) are computed via finite element simulations. In the present case, the commercial (implicit) finite element code used is Abaqus standard [9]. It is driven by the measured displacements (via FE DIC) on the upper and lower edges of the considered region of interest to compute the displacement fields and reaction forces. If the FE mesh is finer in Integrated DIC in comparison to DIC, the measured displacements on the coarser mesh are interpolated on the finer mesh according to the measurement discretization. A Gauss–Newton procedure is implemented to minimize the global functional by iteratively updating the material parameters [18].

2.3. Sensitivity analysis

To probe the identifiability of the seven parameters, a sensitivity analysis is carried out. Consequently, the Hessian of the Integrated DIC code is analyzed [12]. Figure 1(a) shows the global Hessian (H_{IFDIC}) of the IDIC procedure. The material parameters having the largest influence are H_1, H_2, and H_3 and account for the anisotropic plasticity behavior (H_1 is analyzed to show its correlations with other parameters, but for identification purposes its value is kept equal to one half). This result shows that a uniaxial experiment enables for the characterization of an anisotropic behavior. It also indicates that this behavior must be accounted for when plastic anisotropy is suspected to occur. Figure 1(b) shows that the Poisson's ratio is correlated with H_1, H_2, and H_3, and explains why it is necessary to have a model that separates both contributions from Poisson's ratio and the anisotropic coefficients. Once the lowest eigenvalue of the complete Hessian has been taken out, its condition number is of the order of 10^5, which is not too high given the number of remaining parameters. From this analysis, it is concluded that the seven parameters are identifiable.

3. Parameter identification

The present study investigates the mechanical behavior of a 70-µm thick sheet of precipitation hardened stainless steel (17-7 PH grade) in TH1050 condition. The manufacturer [21] assessed the elastic properties of the studied material. The

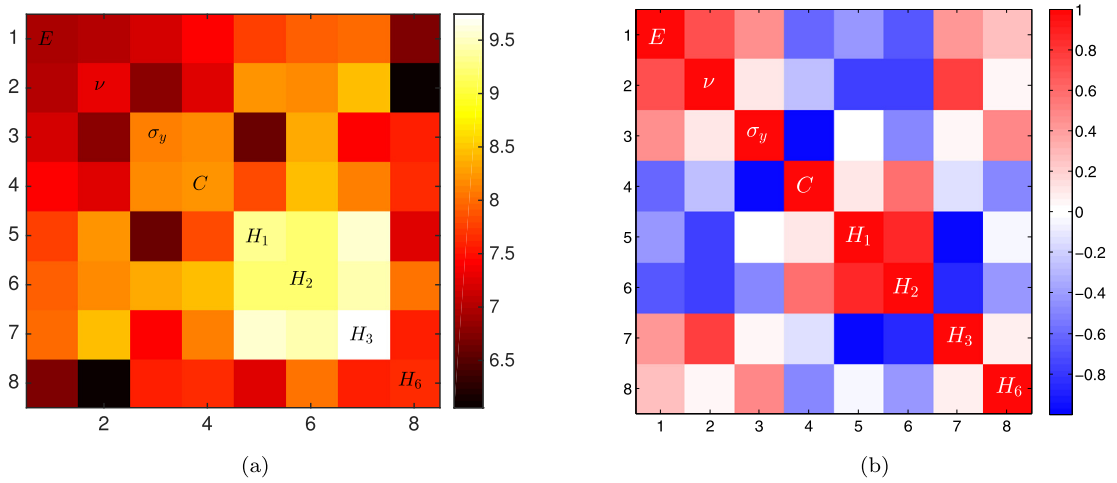

Fig. 1. Global Hessian (a) and its corresponding correlation matrix (b) for the investigated model (i.e. $\{\boldsymbol{p}\} = \{E, \nu, \sigma_y, C, H_1, H_2, H_3, H_6\}^t$). The absolute value of the Hessian is used to allow for a logarithmic scale.

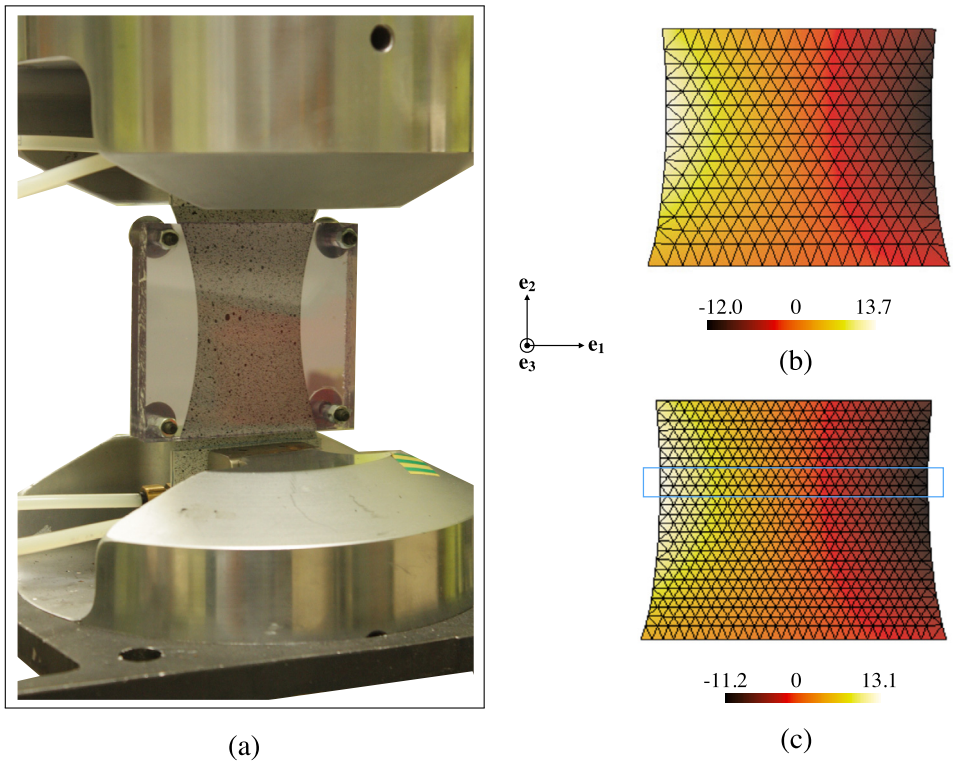

Fig. 2. (a) Uniaxial specimen with dedicated anti-wrinkling device. (b) DIC and (c) IDIC displacement fields u_x at the last experimental time step with two mesh sizes; (c) also shows the area that will be used to assess the Lankford coefficient. The displacements are expressed in pixels (1 pixel $\leftrightarrow$ 70 µm).

specimen is loaded in a servo-hydraulic tension/compression testing machine (see Fig. 2(a)). The experiment consists of three loading/unloading cycles in a displacement controlled mode with increased displacement amplitudes for each new cycle. The unloading phases are stopped when the measured load reaches 10 N to avoid compression. The maximum von Mises equivalent strain is of the order of 8%. 14-bit gray scale images are captured with a digital camera (pco.pixelfly) and a telecentric lens. The effective magnification is 70 µm per pixel. Last, the load measurements and the image acquisitions are synchronized.

The main experimental challenge concerns the specimen thickness that prevents grooved grips to be used. The solution consists in bonding the specimen ends to flat-surface aluminum alloy tabs with a 3M Scotch-Weld Structural Adhesive Film AF 126 [22]. Residual wrinkles are generated during this process near the edges. To maintain the surface flat in the center region (crucial to perform 2D-DIC analyses), an anti-wrinkling device is designed (see Fig. 2). It consists in holding the specimen between two Plexiglas sheets fastened with four screws. A very small gap is left between the Plexiglas sheets to minimize as much as possible the effects of friction on the tested sample. To perform DIC analyses, a random speckle pattern is applied on the monitored surface and no paint loss was observed during the test, thereby validating the hypothesis of negligible friction induced by the anti-wrinkling device. Figure 2 shows at the last experimental time step the measured (b) and identified (c) displacement fields associated with three-nodded triangular meshes with linear interpolation (T3). For DIC, the mesh size is of the order of 60 pixels, and 40 pixels for Integrated DIC.

Figure 3(a) shows the normalized gray level residuals (i.e. χ_f) at each time step for DIC and IDIC analyses. Prior to starting the experiment, 10 images and load measurements are acquired to assess the uncertainties. Then, the experiment starts and the residual increases to roughly four times the noise level. The DIC residual remains relatively constant over the experiment. Conversely, the IDIC residuals are on average higher than DIC residuals. Let us stress that DIC is based on a number of degrees of freedom equal to 600 per image, or 114,600 for the entire experiment, whereas the IDIC approach has no more than seven degrees of freedom. This very drastic reduction incorporates many constraints due to an a priori assumption on the material behavior. The difference in residuals from DIC to IDIC is an indication of the model error that is due to the specific chosen constitutive law. Once the elastic regime ends ($t \geq 20$ s), the IDIC residuals increase and exceed the DIC residuals. This result shows that the assumption of a constant anisotropic behavior, i.e. constant anisotropic coefficients as a function of the plastic strain, is not totally consistent with the experimental data. Similarly, Fig. 3(b) shows that the load levels are consistent in the elastic regime and gradually degrade in anisotropic plasticity.

Table 1 gathers the assessed material parameters for the studied constitutive law. Their initial values ($\{\boldsymbol{p_0}\}$) are chosen according to literature data [21,23]. The initial and last values of the residuals are also shown (1st–last) for the investigated law plus one identification with a coarser mesh (referred to as IDIC*). All the parameters converge to a stabilized level

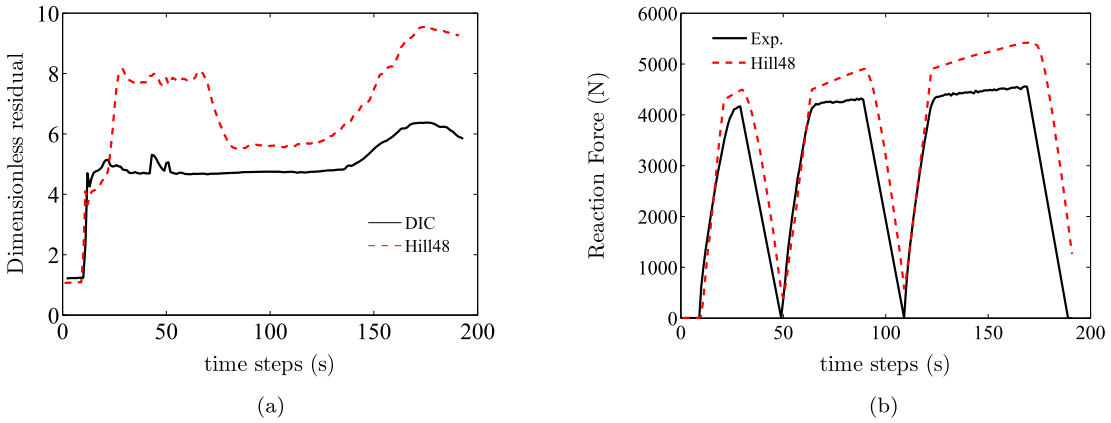

Fig. 3. (a) Gray level residual history $\chi_f(t)$ for DIC and IDIC. (b) Applied and computed reaction force history.

Table 1
Identified parameters and identification residuals via IDIC over the entire loading history cycle (IDIC* corresponds to the DIC mesh and "1st–last" corresponds to the first and last values of the residuals).

	χ 1st–last	χ_f 1st–last	χ_F 1st–last	E GPa	ν	σ_0 MPa	C GPa	H_2	H_3	H_6
p_0		5.0		200	0.3	1300	10	0.5	0.5	1.5
IDIC	11.3–7.0	11.3–7.0	15.5–9.30	202	0.30	1420	9.1	0.42	0.44	1.59
IDIC*	11.1–7.8	11.1–7.8	15.5–10.8	202	0.3	1390	9.2	0.44	0.45	1.56

while the residuals χ for each law are minimized. First, the IDIC residual is greater than the DIC residual obtained with a coarse mesh (i.e. the one used to measure the boundary conditions), but lower than the IDIC* residual obtained on the same mesh. This is an indication that model errors occur. It proves that refining the mesh (Fig. 2) can enhance the identification quality by decreasing the gray level residuals. This mesh difference also explains why the DIC residual is larger than the IDIC residuals during the first time steps ($t \in [10; 20]$ s). The load residuals also decrease.

The lowest global residual corresponds to seven times the noise level, which indicates that the model does not fully capture all the experimental behaviors. Figure 4 shows the displacement field residual for the transverse component (i.e. the difference between the IDIC and DIC displacement fields). The displacement difference is not noise (i.e. measurement uncertainty), but rather a smooth component that is not totally accounted for by the model. This is a clear manifestation of model error. The short wavelength component close to the upper edge is believed to be due to small wrinkles.

The Lankford coefficient is an indicator used to describe the anisotropic plasticity behavior of sheet metals [10]. It corresponds to $r = \epsilon^{\mathrm{p}}_{33}/\epsilon^{\mathrm{p}}_{11}$, where $\epsilon^{\mathrm{p}}_{11}$ is the transverse plastic strain, $\epsilon^{\mathrm{p}}_{33}$ the out-of-plane plastic strain. This analysis is performed in the central area (see Fig. 2(c)) of the specimen and the reported strains are the corresponding mean values. Figure 5 shows the Lankford coefficients both for DIC and IDIC results. For DIC analyses, the elastic strains are evaluated from the applied load and the knowledge of the elastic properties of the alloy. Incompressibility is assumed for the plastic strains

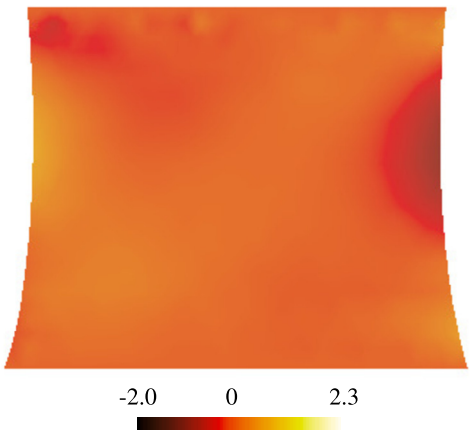

Fig. 4. Transverse displacement field residual (IDIC–DIC) expressed in pixels (1 pixel ↔ 70 µm). Its corresponding root mean square level is equal to 0.19 pixel.

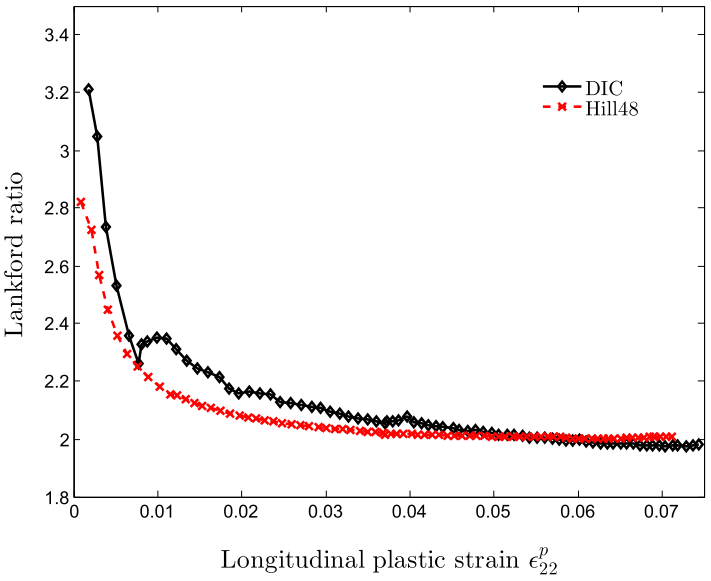

Fig. 5. Lankford ratio evaluated from DIC and from the identified anisotropic elastoplastic model.

to evaluate ϵ_{33}^{p}. The coefficient converges for both cases toward a constant value as the level of plastic strain increases. The asymptotic value (i.e. about 2) is consistent with literature data of cold-rolled stainless steel [24]. Second, the model does not fully capture the experimentally observed anisotropy in the early stages of plasticity. This result shows that even if the identification of the anisotropic coefficients has been achieved, the assumption of a constant anisotropic behavior is an approximation. This is consistent with the fact that the IDIC residuals are higher at the end of cycle 1 and the beginning of cycle 2 (see Fig. 3).

It is to be emphasized that using full field measurements allows for the calibration of the entire set of parameters using a *single* experiment. Such a conclusion was also drawn for a thicker sample made of aluminum alloy [25]. It also gives access to an evaluation of a significant model error (based on the value of the final residuals being well above 1, see Table 1), and it provides in addition an assessment of the deviation in the observed and fitted strains through the Lankford ratio, which may help enriching the constitutive law (say with an evolving anisotropy) in order to reduce the model error.

4. Conclusion

The identifiability of the Hill-1948 model has been investigated with Integrated Digital Image Correlation for a uniaxial test on ultra-thin sheet made of precipitation hardened stainless steel. A dedicated anti-wrinkling system was designed and employed to prevent non-uniform out-of-plane displacements while loading and unloading the specimen. The identification is performed over the entire history accounting for three loading/unloading cycles. The sensitivity analysis proves that the anisotropic yield criterion can *a priori* be quantitatively evaluated. It is shown *a posteriori* that it is possible to determine *all* material parameters for the in-plane anisotropic plastic model in a *single* uniaxial experiment thanks to full-field measurements. Moreover, the same experimental procedure is rich enough to indicate a model error and provides some insight into directions for the enrichment of the constitutive law to better describe the experiment.

Acknowledgments

The authors acknowledge the help of Dr. Hugo Leclerc in the implementation of the DIC codes. This work was supported by the “Région Île-de-France” (THERMOFLUIDE-RT project) and BPI France (DICCIT project).

References

[1] R. von Mises, Mechanik der festen Körper im plastisch-deformablen Zustand, Nachr. Ges. Wiss. Goett., Math.-Phys. Kl. 1913 (1913) 582–592.
[2] R.L. Whiteley, The importance of directionality in deep drawing quality sheet steel, Trans. Amer. Soc. Met. 52 (1960) 154.
[3] D.H. Lloyd, Metallurgical engineering in the pressed-metal industry, Sheet Met. Ind. 39 (1962) 82–91.
[4] W.T. Lankford, S.C. Snyder, J.A. Bausher, New criteria for predicting the press performance of deep drawing sheets, Trans. Amer. Soc. Met. 42 (1950) 1197–1205.
[5] R. Hill, A theory of the yielding and plastic flow of anisotropic metals, Proc. R. Soc. Lond. Ser. A 193 (1033) (1948) 281–297.
[6] J.E. Dorn, Stress–strain rate relations for anisotropic plastic flow, J. Appl. Phys. 20 (1949) 15–20.
[7] R. Hill, Continuum micro-mechanics of elastoplastic polycrystals, J. Mech. Phys. Solids 13 (2) (1965) 89–101.
[8] S. Soare, J.W. Yoon, O. Cazacu, F. Barlat, Applications of a recently proposed anisotropic yield surface to sheet metal forming, in: Advanced Methods in Material Forming, Springer, Berlin, 2007, pp. 131–149.

[9] Abaqus Analysis, User's Manual, Version 2016, Dassault Systems, 2016.
[10] ASTM E517-00. Standard test method for plastic strain ratio r for sheet metal, ASTM International, West Conshohocken, PA, USA, 2010, pp. 1–8.
[11] M. Grédiac, F. Hild (Eds.), Full-Field Measurements and Identification in Solid Mechanics, ISTE–Wiley, 2012.
[12] M. Bertin, F. Hild, S. Roux, Optimization of a biaxial tensile specimen geometry for the identification of constitutive parameters based upon full field measurements, Strain 52 (4) (2016) 307–323.
[13] F. Hild, S. Roux, Measuring stress intensity factors with a camera: integrated digital image correlation (I-DIC), C. R. Mecanique 334 (1) (2006) 8–12.
[14] H. Leclerc, J.N. Périé, S. Roux, F. Hild, Integrated digital image correlation for the identification of mechanical properties, in: Lect. Notes Comput. Sci., vol. 5496, Springer, Berlin, 2009, pp. 161–171.
[15] J. Réthoré, A fully integrated noise robust strategy for the identification of constitutive laws from digital images, Int. J. Numer. Methods Eng. 84 (6) (2010) 631–660.
[16] J. Réthoré, X. Muhibullah, T. Elguedj, M. Coret, P. Chaudet, A. Combescure, Robust identification of elasto-plastic constitutive law parameters from digital images using 3D kinematics, Int. J. Solids Struct. 50 (1) (2013) 73–85.
[17] F. Mathieu, H. Leclerc, F. Hild, S. Roux, Estimation of elastoplastic parameters via weighted FEMU and integrated DIC, Exp. Mech. 55 (1) (2015) 105–119.
[18] M. Bertin, F. Hild, S. Roux, F. Mathieu, H. Leclerc, P. Aimedieu, Integrated digital image correlation applied to elastoplastic identification in a biaxial experiment, J. Strain Anal. Eng. Des. 51 (2) (2016) 118–131.
[19] F. Hild, A. Bouterf, L. Chamoin, H. Leclerc, F. Mathieu, J. Neggers, F. Pled, Z. Tomičević, S. Roux, Toward 4D mechanical correlation, Adv. Model. Simul. Eng. Sci. 3 (1) (2016), 26 pp.
[20] W. Prager, A New Method of Analyzing Stresses and Strains in Work-Hardening Plastic Solids, Technical report, Brown University, Division of Applied Mathematics, 1955.
[21] AK-Steel. Mechanical characteristics 17-7 PH steel, 2013.
[22] 3M, Structural Adhesive Film, AF 126-AF 126 FR, Technical report, 3M, 2002.
[23] A. Leybold-Herbert, Axial-Load Fatigue Tests on 17-7 PH Stainless Steel Under Constant-Amplitude Loading, NASA TN D-439 62 71013, Langley Research Center, Langley Field, VA, USA, October 1960.
[24] G. Charca Ramos, M. Stout, R.E. Bolmaro, J.W. Signorelli, P. Turner, Study of a drawing-quality sheet steel. I: stress/strain behaviors and Lankford coefficients by experiments and micromechanical simulations, Int. J. Solids Struct. 47 (17) (2010) 2285–2293.
[25] J. Neggers, F. Mathieu, F. Hild, S. Roux, N. Swiergiel, Improving full-field identification using progressive model enrichments, Int. J. Solids Struct. (2017), http://dx.doi.org/10.1016/j.ijsolstr.2017.03.013, in press.